# We are IntechOpen,
# the world's leading publisher of
# Open Access books
# Built by scientists, for scientists

## 6,900
Open access books available

## 186,000
International authors and editors

## 200M
Downloads

## 154
Countries delivered to

Our authors are among the

## TOP 1%
most cited scientists

## 12.2%
Contributors from top 500 universities

**WEB OF SCIENCE**™

Selection of our books indexed in the Book Citation Index
in Web of Science™ Core Collection (BKCI)

# Interested in publishing with us?
# Contact book.department@intechopen.com

Numbers displayed above are based on latest data collected.
For more information visit www.intechopen.com

# Transparent Vacuum Insulation Panels

*Takao Katsura*

## Abstract

New, low-cost transparent vacuum insulation panels (TVIPs) using structured cores for the windows of existing buildings are proposed. The TVIP is produced by inserting the structured core, the low-emissivity film, and the adsorbent into the transparent gas barrier envelopes. In this chapter, the authors introduce the outlines, the design and thermal analysis method, the performance evaluation (test) method. Firstly, five spacers, namely peek, modified peek, mesh, silica aerogel, and frame, are selected as the structured core. The effective thermal conductivity of TVIPs with five different spacers is evaluated at different pressure levels by applying numerical calculation. The result indicated that TVIPs with frame and mesh spacers accomplish better insulation performance, with a center-of-panel apparent thermal conductivity of $7.0 \times 10^{-3}$ W/m K at a pressure of 1 Pa. The apparent thermal conductivity is the same as the value obtained by the simultaneous evacuation thermal conductivity measurement applying the heat flux meter method. Furthermore, using a frame-type TVIP with a total thickness of 3 mm attached to an existing window as a curtain decreases the space heat loss by approximately 69.5%, whereas the light transparency decreases to 75%.

**Keywords:** transparent vacuum insulation panels, structured core, retrofitting insulation, design and numerical analysis, thermal conductivity measurement

## 1. Introduction

Environmental issues and the global energy needs have become the most crucial world concerns. This is because of the yearly increase in the annual energy consumption, in addition to the acceleration in the environmental pollution amount. Therefore, several energy-saving thermal insulation techniques have been applied for building applications in new established buildings. On the other hand, the old historical buildings are often protected due to their contributions to society. These thermal insulating technologies are rarely installed to the existing buildings. That is why the insulation capability of the existing buildings is not high. Consequently, it is a mandatory to enhance the insulation performance for the existing buildings. Vacuum insulation panels (VIPs) can be used for this aim. The VIPs have a very low thermal conductivity [1]. Therefore, they considered as a promising method for enhancing the thermal insulation of buildings, specifically for energy retrofitting (where higher insulation performance and smaller thicknesses are desirable) [2]. Further, it is indispensable to decline winter heat loss or heat gain in summer season for the windows of the existing buildings without much affecting the window transparency. The significant decrease in the window transparency increases the daytime energy consumption for the lighting purposes [3].

The research on VIPs has been applied in some fields to improve insulation performance. For example, in some buildings, it can attain five times higher insulation values than conventional building insulating materials [4]. Recently, the common manufactured VIPs are applied for building walls insulation. These VIPs have an opaque appearance. These VIPs structures contain a metallized aluminum film. This aluminum envelope contains a high thermal insulation material under vacuum conditions and placed between the structure layers of a building wall.

Silica powder has been applied for the trial manufacture of VIPs. A silica aerogel with a thermal conductivity of $2 \times 10^{-2}$ W/m K is usually used to make transparent VIPs [5]. It has been found that using such material in smart windows decreases the U-values by 63% as compared to conventional glass windows. In addition, a significant reduction in the light transmittance (by approximately 30%) has been measured [5]. Moreover, the industrial production cost of a VIP using silica aerogel remains very high. Hence, there is a need to search for another economically competitive material.

A new slim structured-core and transparent insulation method for windows of existing buildings is proposed. The TVIP is produced by inserting the structured core, the low emissivity film, and the adsorbent into the transparent gas barrier envelopes. In this chapter, the authors firstly describe the outlines of TVIPs. Next, the core structural design to maintain a vacuum layer and the thermal analysis method to predict the insulation performance are explained. In addition, measurement methods of apparent thermal conductivity and light transmittance, which are used to evaluate the insulation performance and transparency of TVIPs, are introduced. Furthermore, the results of thermal performance analysis and annual energy analysis are demonstrated.

## 2. Outlines of transparent vacuum insulation panels

### 2.1 Outlines, applications, and advantages

**Figure 1** shows a concept diagram of the TVIP [6]. The manufacturing steps start with the preparation of the VIP core structure, transparent low-emissivity (Low-E) sheet, and transparent envelope. The heat sealing of the envelope is a four-sided seal type. In addition, the Low-E film coated on one face, whereas the other face has a larger emissivity. The core structure and the Low-E film are inserted in a transparent gas barrier envelope. In addition, the oxide calcium adsorbent pack or the getter material is also inserted to adsorb the outgassing from core material and the gas passing through the envelope. The transparent envelope facilitates the applicability of these TVIPs to existing windows where light transparency is
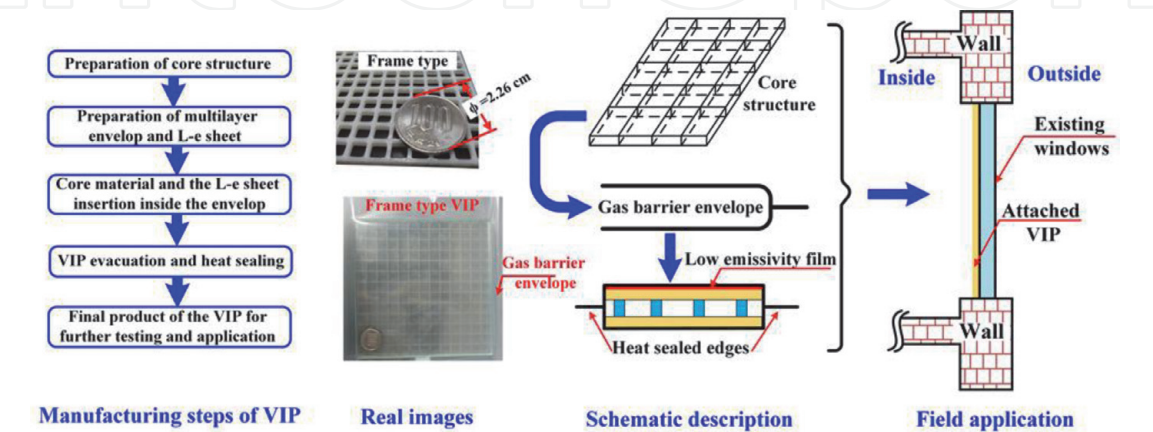


**Figure 1.**
*Manufacturing steps, real images, schematic description, and the proposed real field application of the structured-core and transparent vacuum insulation panel (TVIP) for existing windows [6].*

indispensable. The full structure is evacuated and sealed in a vacuum sealing machine after reaching the vacuum design pressure. **Figure 2** shows an example of lab-scale vacuum sealing machine [6]. In this machine, the pressure level can be controlled either automatically or manually. After reaching the desired pressure, sealing is automatically performed. Then, the sample can be taken from the vacuum chamber. The vacuum sealing machine usually consists of a few vacuum pumps (the vacuum sealing machine shown in **Figure 2** has buster and rotary vacuum pumps.). Also, the sealing can be achieved by a machine.
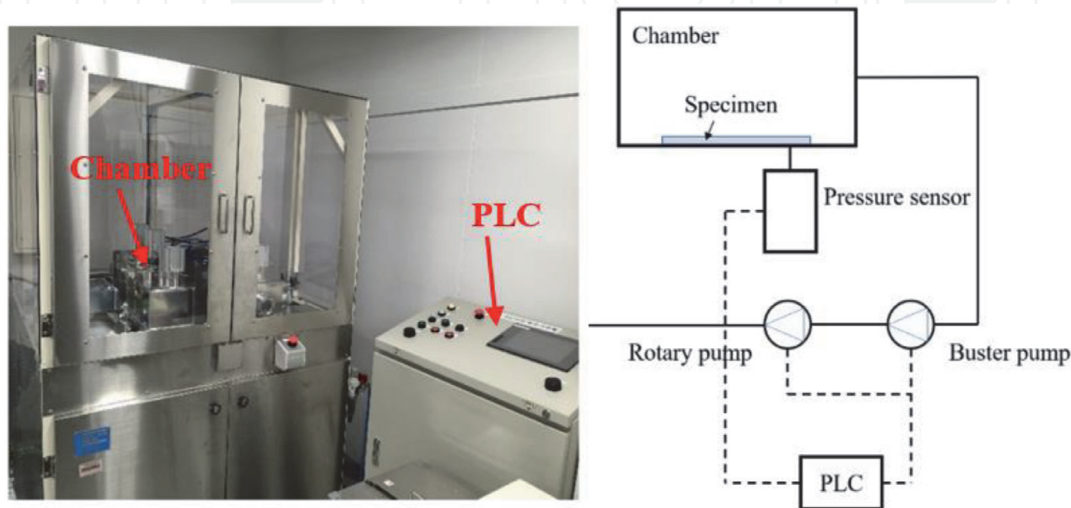
Usually, a sealing with approximately 10 mm width are used to prevent the penetration of atmospheric pressure. **Figure 1** depicts the real appearance, schematic illustration, and the method used for the field applications for the proposed VIPs. These VIPs might contribute to enhance the insulation capability of current existing windows, with slight effect on the daytime light transparency. These VIPs can be integrated as transparent curtains with low thermal conductivity and small thickness.

The advantage of TVIPs applying the structured core materials compared with the conventional transparent insulation technologies such as the vacuum glazing and the TVIP using silica aerogel is low cost to produce. **Figure 3** presents the comparison of costs [6]. The total TVIPs cost including envelope, inner spacers, and film of Low-E coating are shown in **Table 1** [6]. It is obvious that the cost of VIPs is around one-third of using double-glazing with vacuum. Further, the currently proposed VIPs can be attached to the existing windows with lower installation cost compared to silica aerogel VIPs. Finally, the cost of L-e film is around 50% of the total VIP price.
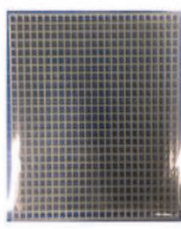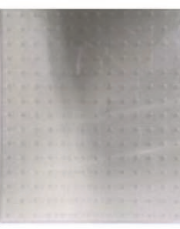
## 2.2 Core materials

The structure core materials are required the following items.

1. Strong enough to maintain a vacuum layer against atmospheric pressure from outside of envelope.

2. Low thermal conductivity to reduce the thermal bridge generated by the core materials.

3. No outgassing after vacuum sealing.

4. Easy to manufacture and inexpensive.



**Figure 2.**
*Photograph and schematic of the vacuum sealing equipment [6].*

| Real photos |  |  |  |  |  |
|---|---|---|---|---|---|
| Design | Double-layered vacuum glazing | Frame VIP | Mesh VIP | Silica aerogel VIP | Pillar supported VIPs |
| Total Cost | > 270 $ + (90 $ construction fee) | < 99 $ | < 90 $ | > 4500 $ | < 135 $ |

**Figure 3.**
*Comparison of the calculated production cost of proposed VIPs with the double-layered vacuum glazing insulation [6].*

| Item | Mesh spacer | Frame spacer | Peek spacer | Silica aerogel |
|---|---|---|---|---|
| Core material | 9 $ | 18 $ | 36 $ (plates + pillars) | 4401 $ |
| L-e film | 45 $ | 45 $ | 45 $ | 45 $ |
| Envelope | 18 $ | 18 $ | 18 $ | 18 $ |
| Manufacturing fee + adsorbent | 18 $ | 18 $ | 36 $ | 36 $ |
| Total cost | 90 $ | 99 $ | 135 $ | 4500 $ |

**Table 1.**
*Detailed costs of the manufactured VIPs ($/m$^2$) [6].*

The structured core materials used for TVIPs are depicted in **Figure 4** [6]. These TVIP designs include a peek spacer, mesh spacer, frame spacer, modified peek spacer, and silica aerogel spacer. All of these VIPs are designed, manufactured, and experimentally tested, except for the modified peek spacer. The modified peek spacer is proposed as extensions for the peek spacer. The TVIPs with peek spacers and aerogel spacers are superior to the TVIPs using a frame spacer and a mesh spacer from the viewpoint of transparency. On the other hand, the VIPs using a frame spacer and a mesh spacer have an advantage that it is easy to manufacture. In particular, if the frame spacer can be mass-produced at low cost, it is considered to be the most promising core material for the TVIP.

## 2.3 Envelopes

Metalized film barrier envelopes are commonly used in the conventional VIPs; however, they cannot be applied to the TVIPs. Transparent gas barrier films are applied as a covering envelope for the structured core. These envelopes are favorable for sealing and transparency. **Figure 5** depicts one example of detailed structure and dimensions of the transparent gas barrier envelope [6]. In order to reduce the oxygen and moisture transmission rates, the silica evaporated PET layer is applied.
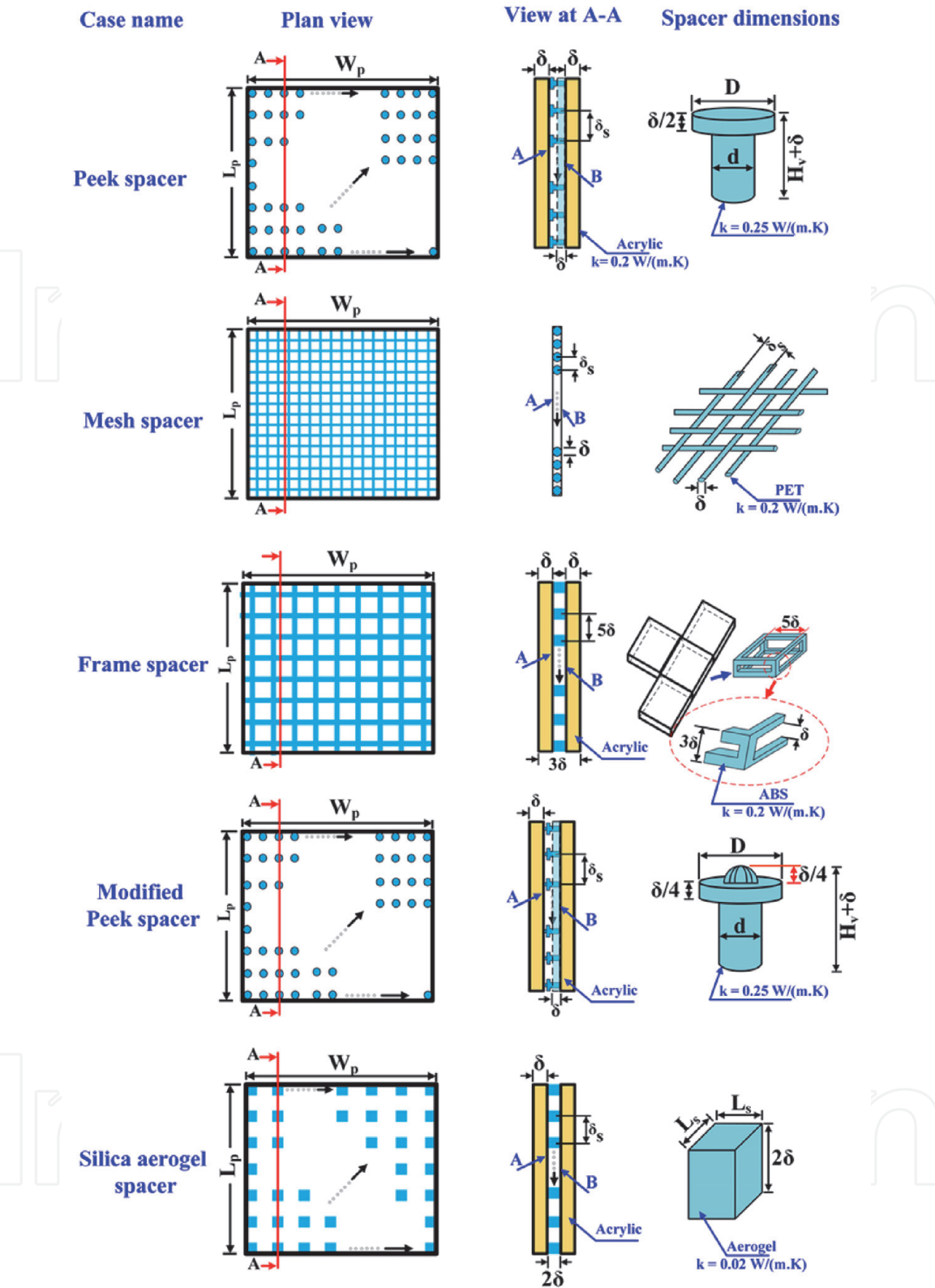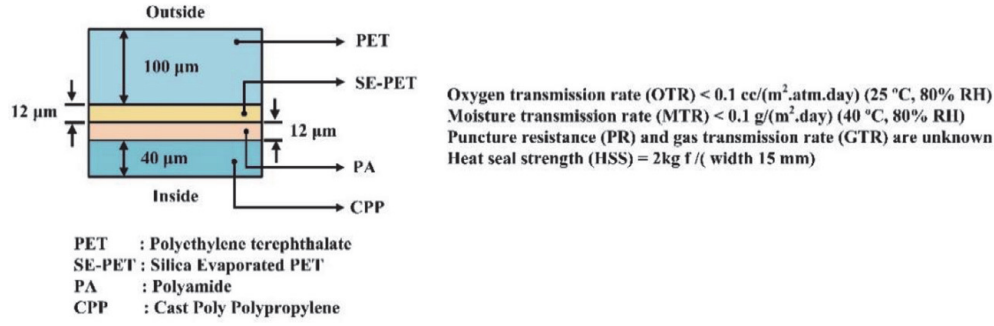
**Figure 4.**
*Concept diagram of the proposed structured-core and transparent VIPs with different core structures of peek spacer, mesh spacer, frame spacer, modified peek spacer, and silica aerogel spacers [6].*

## 3. Design and thermal analysis of transparent vacuum insulation panels

### 3.1 Core structural design

In order to determine the reasonable size of the VIP, the stress analysis is required. In this chapter, an example of stress analysis for frame spacer is

**Figure 5.**
*One example of detailed structure of the transparent gas barrier envelope [6].*

demonstrated. The structural frame depicted in **Figure 6** (on the left) [7] is used to maintain a vacuum gap when the internal pressure is decreased to 0.1 Pa. This clarifies that every frame should hold up an atmospheric pressure loading. The representation is shown in **Figure 6** (on the right) [8, 9]. The structural calculation analysis conducted to a model in **Figure 7** is separated into two possibilities.

The structural model used in this work is simplified as support beam. The deflection is used to estimate the structural dimensions. The calculation model shows the maximum stress could be happen at the center of the beam and while the minimum stress occurs at the frame edge. In this simulation, when the atmospheric pressure is used as the loading, a compression and elastic occur simultaneously but with opposite directions. Then, a relationship between the span and the deflection is defined using the following equation:
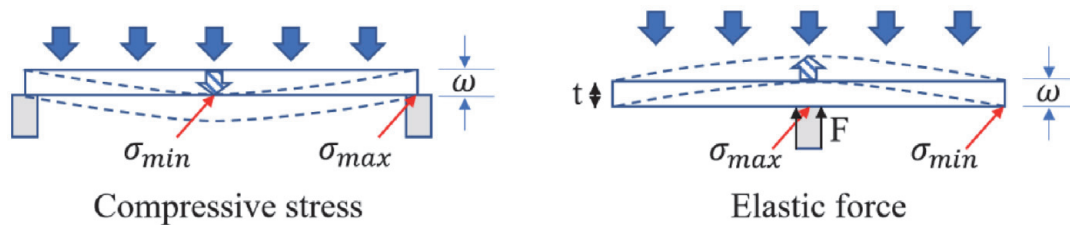
$$\overline{\omega}_{max} = \sigma \times \frac{P_0 \times a^4}{D} \tag{1}$$

$$D = \frac{Et^3}{12(1 - \mu^2)} \tag{2}$$

If the polycarbonate frame is used, the Young's modulus $E$ is 2.32 GPa and the Poisson's ratio $\mu$ is 0.39. The polycarbonate frame width, $t$, is used as 1 mm, while
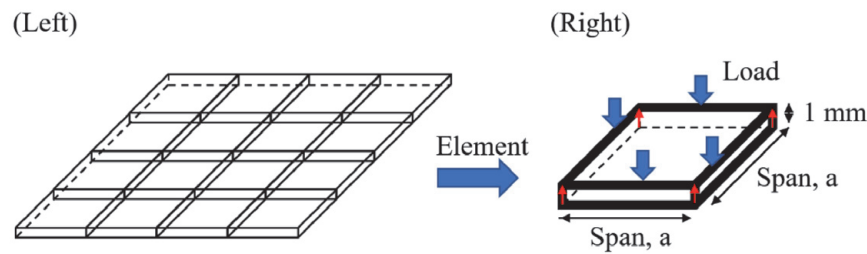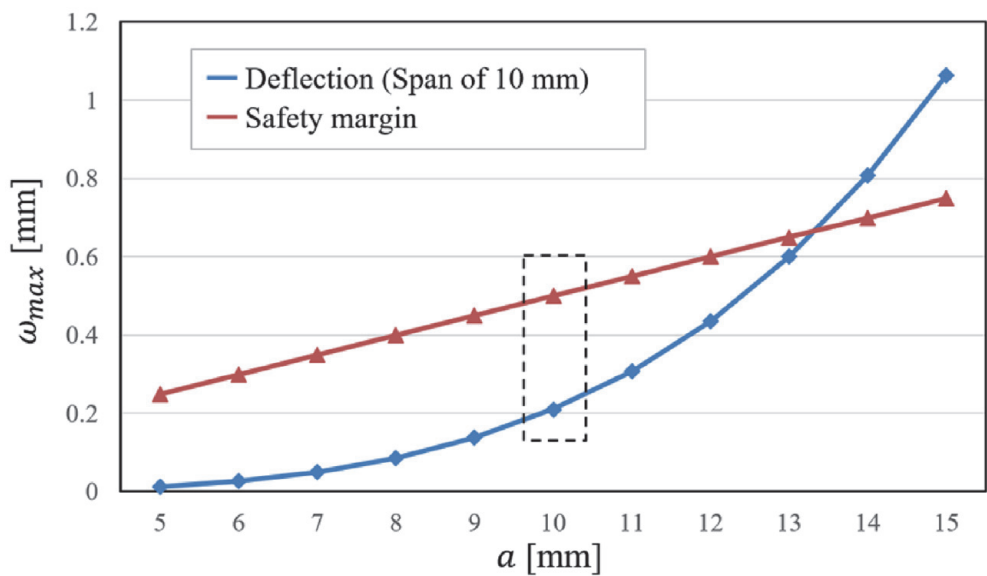


**Figure 6.**
*One example of structure analysis for a frame-structured VIP [7].*



**Figure 7.**
*Representation figures of the proposed structural model [7].*

the span, *a,* is used as10 mm, the uniform loading coefficient to a rectangular flat plate $\sigma_1$ is 0.0138, and $\sigma_2$ is 0.0611. Further, the value of $P_0$ is used to be 1013 kPa. The frame extreme deflection with different spans vales is revealed in **Figure 8** [7]. However, the effect of these structural designs significantly influences the insulation capabilities. In order to create an appropriate design for VIP, we discussed additional models. Therefore, we designed the structure by changing the width of frame from 0.5 to 1.5 mm, and changing the span to 5, 8, 10, 12, and 15. The influence in deflection is revealed in **Figure 9** [7].

The frame mechanical structure is designed within the safety condition is showed in **Figure 8**. The frame span of 10 mm is used, while considering the stress effects and distortion, to used in the numerical model of thermal transmittance and to predict the thermal insulation capabilities of the proposed specimen in the experimental manufacturing. Furthermore, the vacuum gap was attained, and the frame surface was quite flat with a designed span of 10 mm. **Figure 9** compares the deflections at different conditions. The frame design also considered the



**Figure 8.**
*The variation of maximum imposed deflection of the frame design at different span values [7].*
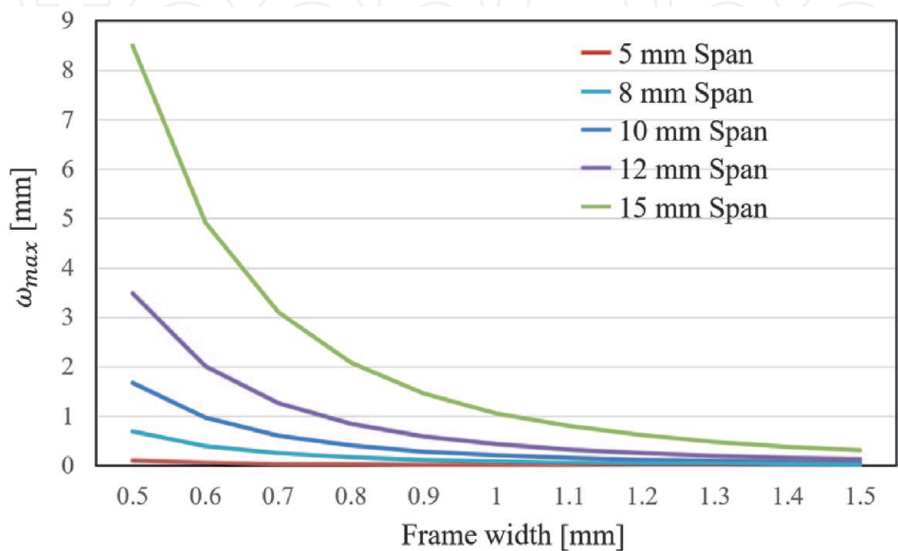


**Figure 9.**
*Variation of the estimated deflections under various design conditions [7].*

transparency along with the insulation performance. Hence, the frame with width of 1 mm, span of 10, and transparent gas barrier envelope is used.

To validate the aforementioned design, a 3D model was developed using ANSYS workbench 14.0. The distribution of deformation for the core frame that is modeled as concept in **Figure 10** and the result is shown in **Figure 11** [7]. The fixed boundary indicates that the element analysis can be applied to a full-scale VIP, and the meshing in **Figure 10** shows the calculation result is accurate due to the 257,791 nodes and 49,046 elements. The result validates the mechanical analysis in **Figure 8**, indicating a reasonable structural design with a sufficiently flat for application.

## 3.2 Thermal analysis applying numerical calculation

In VIPs, the inner pressure must be reduced to below 10 Pa. Increasing the gas pressure above this value rapidly increases the VIP thermal conductivity [10]. In addition, the total heat transfer in VIPs can be divided into four parts: radiation heat transfer through the vacuum space, heat conduction through the skeleton of the core of the core structure, gas conduction, and gas convection [10]. To enhance the insulation performance of the VIP, all of these parts must be minimized. However, at very low pressures, the convection can be naturally converted to pure gas conduction. Therefore, the convection can be ignored in the calculation [11–13]. Hence, the current problem contains a coupled conduction radiation heat transfer. The 3D
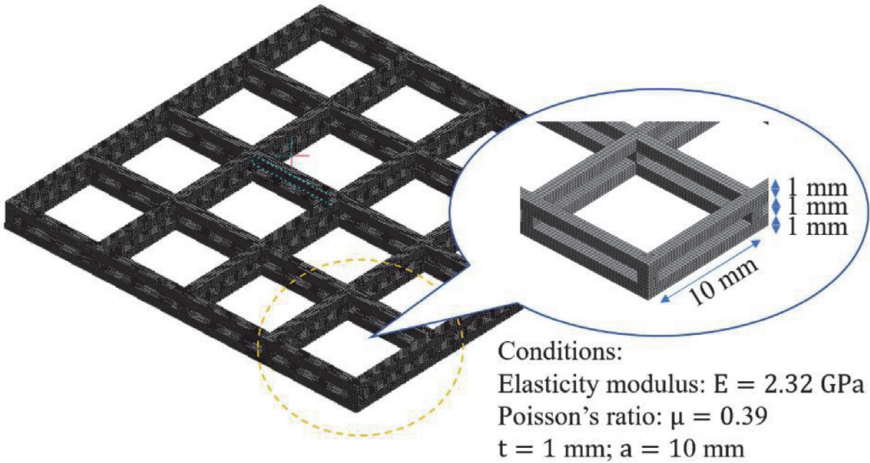


**Figure 10.**
*Three-dimensional meshing stage in finite element model [7].*
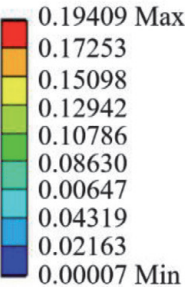


**Figure 11.**
*Distribution of deflection on frame (three-dimensional) [7].*

heat conduction equations for the solid regions including the pillars and in TVIP were coupled with the surface to surface radiation model. The current model adopts the following assumptions:

a. Steady state analysis is conducted.

b. The gas convection effect can be neglected within the simulated vacuum pressure [11, 12].

c. Because the low-emissive films have a very small thickness, the conduction heat transfer in this layer is neglected. But, the effect of its low emissivity is taken into consideration in the radiation heat exchange in the vacuum region.

d. The heat transfer by conduction in the envelope of the TVIP is also ignored.

e. The thermal contact resistances in between the layer structures are negated.

f. Isotropic materials were assumed for the complete structure of the TVIP.

The steady-state 3D energy equation with radiation source term can be written as follows as mentioned in ANSYS FLUENT [14]:

$$\nabla.(k\nabla T) + S = 0 \tag{3}$$

where $T$ is the element temperature, $k$ is the element thermal conductivity, and $S$ is a source term. This term is added to consider the effect of the radiation exchange in the vacuum space [14]. This equation is solved for all solid domains but with zero radiation heat source. Further, the gas conduction can be neglected at lower pressure. But, in this study, the gas thermal conductivity variation with the pressure, gas mean temperature, and vacuum layer thickness is considered in the calculations [15]. In this work, the air thermal conductivity in the vacuum space at different pressure, temperature, and pore size is calculated as follows:

$$\lambda_v = \frac{\lambda_o}{1 + \frac{(1.07\times 10^{-7})T}{l_v P}} \tag{4}$$

where $T$, $l_v$, and $P$ are the gas temperature in K, vacuum layer thickness in m, and pressure of the gas layer in Pa respectively. Further, $k_o$ is the thermal conductivity of the air gap at a reference temperature, which is about 0.026 W/m K.

The radiation exchange is predicted in the TVIP is estimated using the surface to surface (S2S) radiation model existing in ANSYS. This model defines the faces participating in the radiation heat exchange and the view factor is calculated using the surfaces separation, orientation, and the surface size. The surfaces participating in the radiation heat exchange are the surfaces in contact with the vacuum regions [14]. This view factor is identified using the design geometry of the TVIP. Further details, and the S2S model limitations exists in ANSYS theory guide [14].

The boundary conditions used in this study were depicted in **Figure 12** including the schematic representation, boundary conditions, and the meshing details for all the proposed TVIPs [6]. One side of the TVIP is kept at a temperature of 35.5°C, while the other was kept at a temperature of 10.5°C. The wall emissivity and temperature are well defined in the vacuum zones. But, for the spacers, only the faces' temperatures are defined, because the radiation exchange happens only in the vacuum regions. Furthermore, the peripheral edges of the TVIP were assumed to be isolated due to the
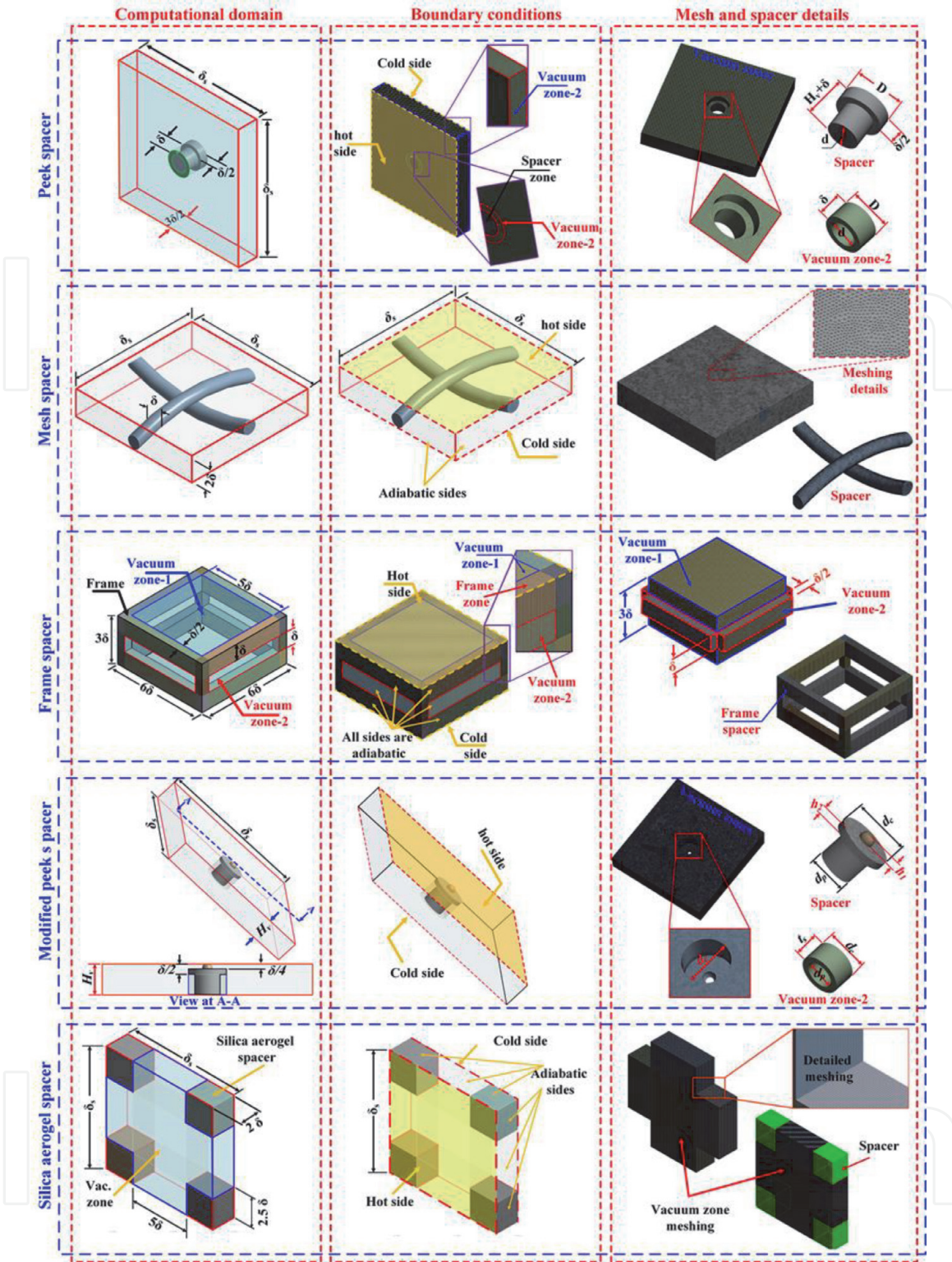
**Figure 12.**
*Computational domains, boundary conditions, and mesh details for all investigated cases [6].*

symmetrical computational domain. Finally, all interfaces in between the layers were thermally coupled. At this condition, the temperature and the heat transfer rate on these interfaces were assumed the same. The boundary conditions are mathematically expressed as follows for the for the frame-type spacer.

- For hot TVIP side:

  At the spacer face $T = T_h$.

  At Vacuum faces $= T_h$; $\varepsilon = \varepsilon_h$.

- For the cold wall:

At the spacer zones $T = T_c$

At the vacuum zones $= T_c; \varepsilon = \varepsilon_c$

Mesh study test is completed to confirm that the predicted results are not dependent on the mesh size. A total number of elements of 1,370,521, 2,450,133, 1,745,551, 864,000, and 1,600,000 were used for the simulation of the peek, modified peek, mesh-type, frame-type, and silica aerogel spacers, respectively.

First, the computational domains were created on the "DesignModular" software several zone approach. In this approach, the computational domain is separated into different zones. This allows us to control of element size, properties, and boundary conditions of every zone individually. Then, the generated domains are meshed as detailed in **Figure 12**. Fluent solver is used to solve the module governing equations. In this module, the flow equations including continuity, momentum, and the energy equation are the standard equations. At very low pressure, the convection effect can be neglected and therefore the fluid flow equations are deactivated [16–18]. But, the S2S model must solved for a fluid domain. So, the vacuum gap is simulated as a fluid zone, but only the energy equation is solved. The S2S model uses the estimated view factors. The energy equation for the solid zones and the vacuum space with the S2S radiation, are concurrently solved. Besides, the radiosity estimation is completed using the calculated view factors. The pressure effect is considered in the calculation by estimating the vacuum region thermal conductivity as a function of the vacuum pressure using Eq. (4). Layers for shell zone conduction are considered in the simulation to consider the effect of acrylic plates' existence.

The predicted center-of-panel thermal conductivity is compared with the measured thermal conductivity obtained by the Experiments for the peek type spacer,
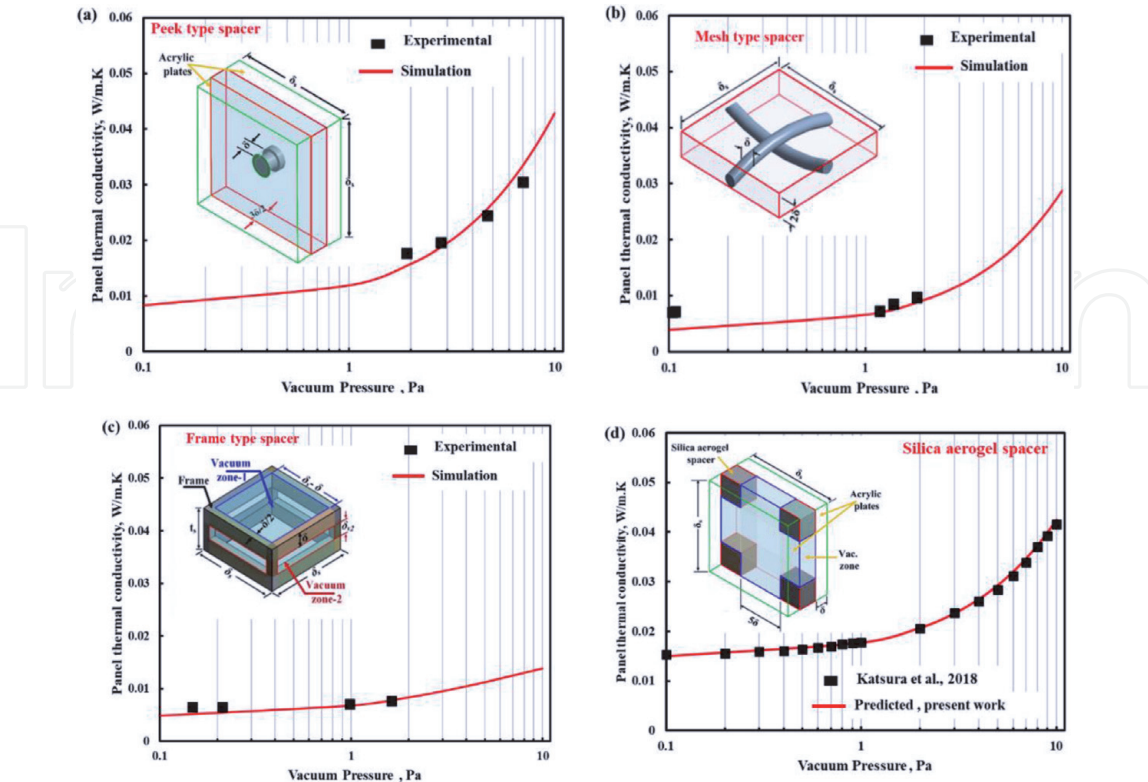


**Figure 13.**
*Comparison of the predicted center-of-panel thermal conductivities with (a) the experimental results for peek spacer; (b) the experimental results for mesh spacers; (c) experimental results of frame-type spacer; and (d) the numerical results of [19].*

mesh-type spacer, and frame-type spacer in **Figure 13a–c**, respectively. The experimental results in **Figure 13a–c** are obtained by the heat flux meter method (simultaneous evacuation thermal conductivity measurement) and the detail of experiment is described in Section 4.1.3. Further, the currently predicted results are compared with the numerical results of [19], as revealed in **Figure 13d**. The current model is inspected at pressure from 0.1 to 10 Pa. The predicted results in **Figure 13a–c** clarified that the model accurately predicts the center-of-panel thermal conductivity for the proposed TVIPs with different core structures with error less than 11%. This error is at lower pressure for the mesh-type spacer because of two reasons. The first reason is that at lower pressure, the contact between the rods become larger due to the flexibility of the rods. This reality is difficult to be considered in the simulation. The second reason may be attributed to the outgassing from the core structure.

Further, the current model is verified for the silica aerogel spacer with the results proposed in [19]. In this part, the silica aerogel spacer dimensions, boundary conditions, and vacuum zone dimensions are the same as those existing in [19], and are displayed inside **Figure 13d**. The main difference between the present model and the model developed by [19] is that the current model is a 3D model that uses S-S radiation, whereas the model developed in [19] was one-dimensional. From **Figure 13d**, a very good agreement is detected.

## 4. Performance evaluation method for transparent vacuum insulation panels

### 4.1 Thermal conductivity

Steady-state thermal conductivity measurement method for a flat material is used to evaluate the thermal insulation performance of TVIP. Two methods are commonly applied. The first one is the guarded hot plate (GHP) method and the second one is the heat flux meter (HFM) method. Of these two methods, the HFM method is recommended to use a standard sample with the same thermal conductivity as the material to be measured and to calibrate the heat flux meter. However, there is no standard sample with a thermal conductivity comparable to the VIPs. Therefore, the GHP method is said to be more suitable for high-precision measurements. Also, if the inside of GHP apparatus can be evacuated, it is possible to obtain the apparent thermal conductivity of TVIP for the set pressure. This means that the GHP method can provide the "ideal" apparent thermal conductivity of TVIP. Meanwhile, the HFM method has the advantage of easy measurement. In addition, the HFM apparatus is inexpensive compared to the GHP apparatus. From these reasons, in recent the HFM method is widely applied compared to the GHP method. Especially, the HFM method is selected when the speed and convenience are required such as quality control.

In the HFM method, TVIPs after vacuum sealing and TVIPs under evacuating can be used. When the TVIP after vacuum sealing is used and the HFM method is applied, the measured apparent thermal conductivity sometimes becomes higher compared to the expected value due to the outgassing from the core material. On the other hand, when the TVIP under evacuating is used and the HFM method is applied (simultaneous evacuation thermal conductivity measurement), it is possible to obtain the measured apparent thermal conductivity of TVIP for the set pressure as well as the GHP method.

In the following, the outlines and examples of each measurement method are introduced.

### 4.1.1 Guarded hot plate method

**Figure 14** shows a schematic diagram of the GHP method. The two specimens, which have the same dimension and density, are positioned between the hot and cold plates and guarded in an airtight chamber. The cold plates are heated such that well-defined, selectable temperature difference ΔT°C is recognized between the two plates. The input heat power Q (W) through an area A (m$^2$) of the hot plate is measured at the thermal equilibrium conditions. Further, the input power, sample thicknesses, temperatures across the sample can be measured and hence the thermal conductivity can be determined at the steady-state conditions. Additionally, this method provides an evacuated space, which is accurate in evaluating the insulation capabilities in a stable vacuum situation. Until reaching the steady-state heat flow and vacuum level, the TVIP thermal conductivity, ($\lambda$), is estimated using the following equation:

$$\lambda = \frac{Q/2A}{\Delta T/d} \tag{5}$$

However, gaps are generated in the evacuated chamber in GHP method. Especially, if the shape of specimen is flat plate and the surface is hard, gaps are generated in the circled area in **Figure 14**. The gaps increase the thermal resistance; therefore, the thermal conductivity of TVIP evaluated by Eq. (5) becomes smaller due to the thermal resistance. Hence, the experimental result should be optimized using the following equation to eliminate the influence of the gaps:

$$R_{VIP} = R_m - R_{Va1} - R_{va2} - R_{va3} \tag{6}$$

where, $R_{Va1}$, $R_{Va2}$, and $R_{Va3}$ are the thermal resistances of each gap. In addition, the apparent thermal conductivity of TVIP can be obtained by the following equation.

$$\lambda_{VIP} = L_{VIP}/R_{VIP} \tag{7}$$

An example of the thermal conductivity measurement applying GHP method, in which a frame structured core shown in **Figure 15** is used as the specimen, is demonstrated [7]. In this measurement, the inside the chamber of the GHP apparatus was reduced to 0.1 and 1 Pa. Then, the thermal conductivity was measured by using GHP method. The experimental results and their optimized results by Eq. (7) are shown in **Table 2** [7]. Furthermore, they are compared with the result of numerical calculation. **Figure 16** illustrates the comparison of apparent thermal
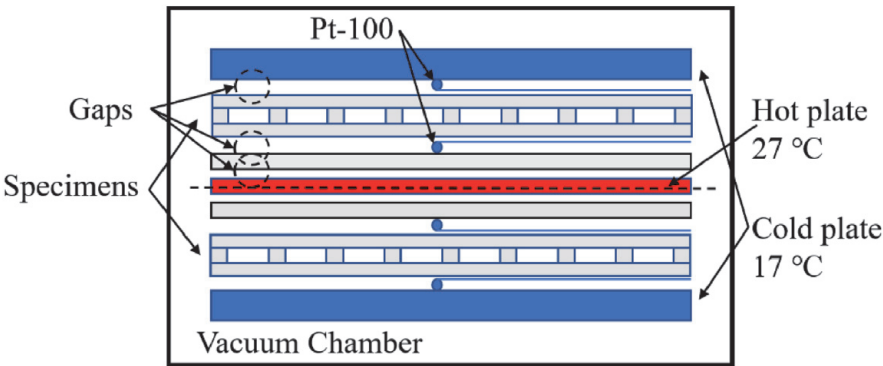


**Figure 14.**
*Schematic of the guarded hot plate apparatus [7].*
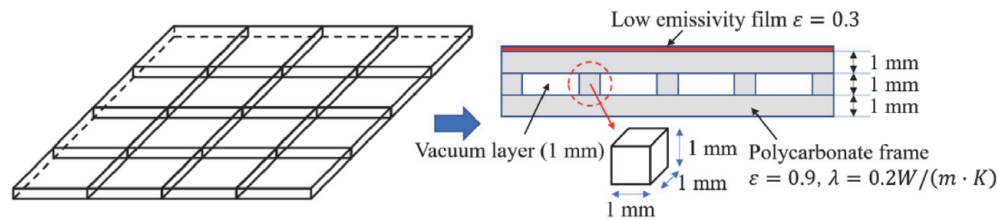
**Figure 15.**
*Concept diagrams of the VIP specimen [7].*

| Pressure (Pa) | Experimental thermal conductivity $\lambda_m$ (mW/(m·K)) | Experimental Thermal resistance $R_m$ ((m²·K)/W) | Thermal resistance of gaps $R_{va}$ ((m²·K)/W) | Thermal resistance of VIP (Optimized) $R_{VIP}$ ((m²·K)/W) | Thermal conductivity of VIP (Optimized) $\lambda_{VIP}$ (mW/(m·K)) |
|---|---|---|---|---|---|
| 0.1 | 2.7 | 2.10 | 0.21 | 1.27 | 4.2 |
| 1 | 3.4 | 1.57 | 0.17 | 0.88 | 6.2 |

**Table 2.**
*Guarded hot plate (GHP) experimental results [7].*

conductivity of TVIP between experiment and calculation [7]. These results indicate that the optimized results are closer to the results of numerical calculation.

### 4.1.2 Heat flux meter method

**Figure 17** shows a schematic diagram of the HFM method. The TVIP specimen is inserted between the hot plate and the cold plate. The temperature of the hot plate and the cold plate can be kept at constant. Then the heat flux is generated by the temperature difference between the hot plate and the cold plate and it is measured by the heat flux meter.

The apparent thermal conductivity of TVIP is measured based on a Fourier equation of one-dimensional heat conduction, as the following:

$$\lambda_{eff,exp} = \left(\frac{q_h + q_c}{2}\right) \times \frac{L_{VIP}}{\Delta T} \tag{8}$$

where the $\lambda_{eff,exp}$, $q_h$, $q_c$, $L_{VIP}$, and $\Delta T$ are the TVIP measured thermal conductivity in W/m K, heat flux measured at the hot and cold sides of the sample
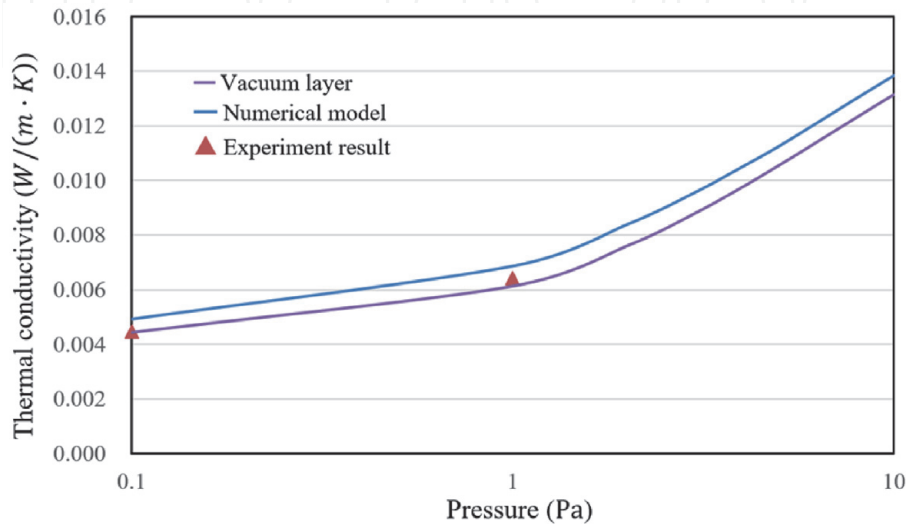


**Figure 16.**
*Comparison of the simulation and experimental results [7].*
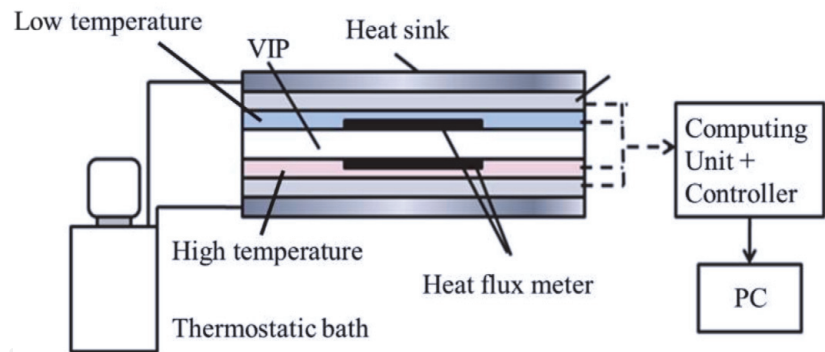
**Figure 17.**
*Schematic diagram of heat flux method apparatus.*

measured using two heat flux sensors in W/m$^2$, the TVIP thickness in m, and the difference in temperatures across the sample sides in °C, respectively.

An example of the thermal conductivity measurement applying HFM method is demonstrated [6]. Four types of core materials (peek spacer, mesh spacer, frame spacer, silica aerogel spacer) are used and the specifications are shown in **Figure 2** and the dimensions are indicated in **Table 3** [6]. The VIPs are produced by inserting the core materials, Low-E film (the emissivity is approximately 0.28), and oxide calcium adsorbent packs into gas barrier envelopes and vacuum sealing. The sealing was performed after the pressure inside chamber was lower than 0.1 Pa. Then, the apparent thermal conductivities of TVIPs were measured by using the heat flux method. **Figure 18** shows the measured apparent thermal conductivity according to elapsed time [6]. The apparent thermal conductivity is increasing according to elapsed time. This issue should occur due to the increased pressure, and the reason should be due to the outgassing from the core material.

In addition, the core material outgassing is minimized in different methods. First, **Figure 19a** [6], called "normal case," the TVIP is assembled by the vacuum sealing machine in **Figure 2**, and a calcium oxide powder placed in an adsorbent pack is used to reduce the core outgassing. Second, in **Figure 19b** [6], called "vacuum drying with N$_2$," all the TVIP components are placed inside an environmentally controlled chamber. In this chamber, the temperature was maintained constant at 70°C for a period of 24 h. After that, the TVIP structure is evacuated using another vacuum machine with turbomolecular vacuum pump to keep the pressure at 0.1 Pa. This could enhance the release of the outgassing from the core material of the TVIP. Then, nitrogen is supplied to the chamber then the nitrogen is exhausted. Finally, the TVIP is evacuated and evacuated and sealed using the machine in **Figure 2**.

| Dimension | Value (mm) | Dimension | Value (mm) |
|:---:|:---:|:---:|:---:|
| $\delta$ | 1 | D | 1.8 |
| $W_p$ | 150 | $L_p$ | 150 |
| d | 1.2 | $H_v$ | 1.5 |
| $\delta_s$ | 10 | $L_s$ | 5 |

**Table 3.**
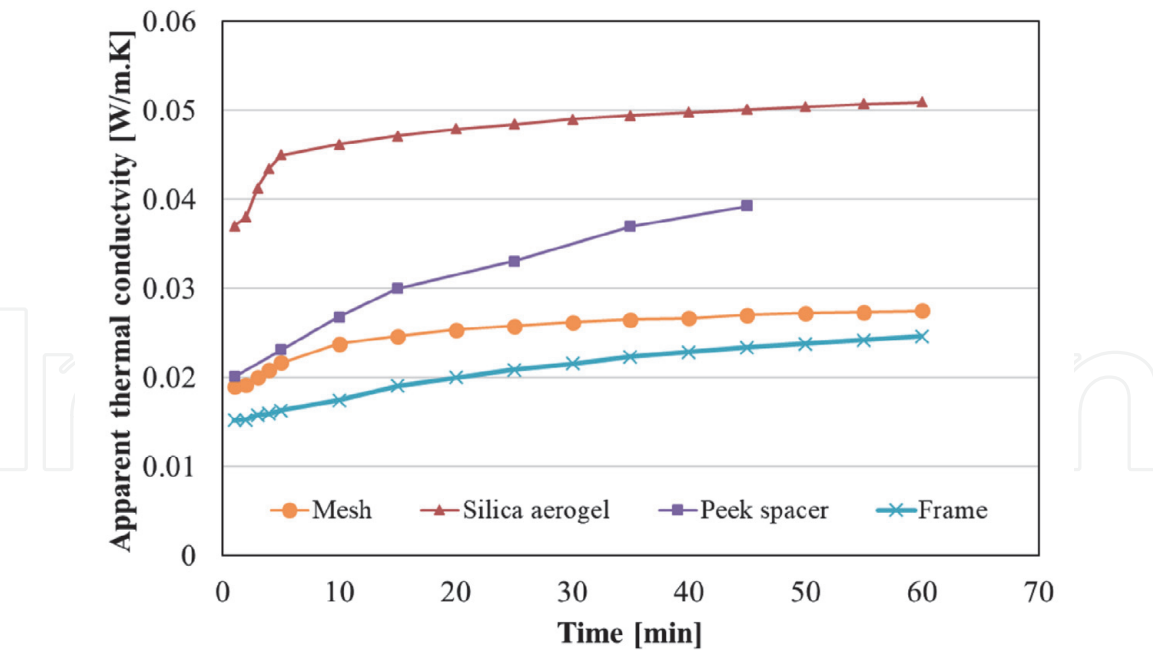*Detailed dimensions of the current structured-core and TVIPs [6].*

**Figure 18.**
*Measured apparent thermal conductivity according to elapsed time [6].*

Third, **Figure 19c** [6], called "heating," a new method is introduced to decrease the production processes used for the fabrication of the TVIP. In this method, heating up the VIP is conducted during the evacuation using two flat silicon rubber heaters. This helps the outgassing during the evacuation. The heaters temperatures were kept at 70°C using controller. In both second and third methods, calcium oxide adsorbent packs were kept inside the TVIP. Finally, in the fourth method displayed in **Figure 19d** [6], called "gas adsorbent getter," a different absorbent material is used. This material contains calcium oxide with alloy getter. The calcium oxide is used to absorb the water vapor and the alloy getter is used to absorb other gases such as nitrogen and carbon dioxide. Therefore, the pressure increase due to the outgassing could be decreased.

In **Figure 20a** [6], the predicted thermal conductivity variation with time is displayed for the four trial production methods. The comparison is executed for the TVIP with frame type. It is found that the use of getter material during the fabrication process achieves the lowest thermal conductivity compared to other methods. Further, manufacturing the VIP without using calcium oxide is the worst option. Because using the getter material attained the best results, further fabrication method is applied here. The use of getter is compared with the use of a calcium
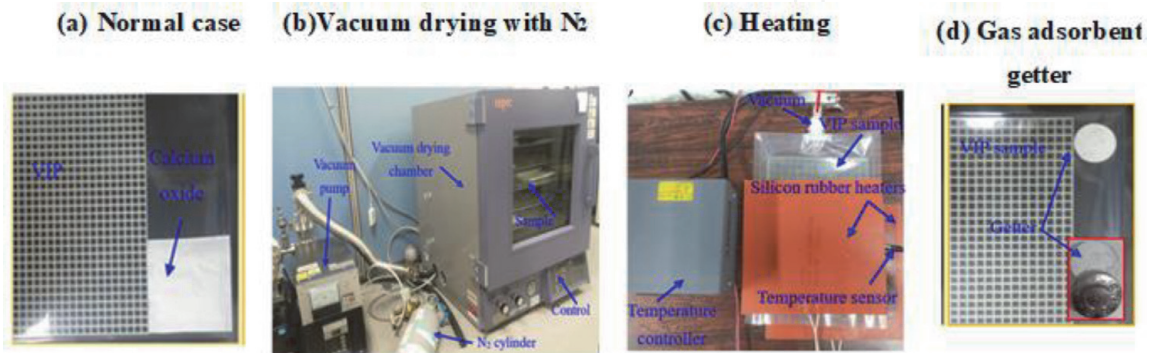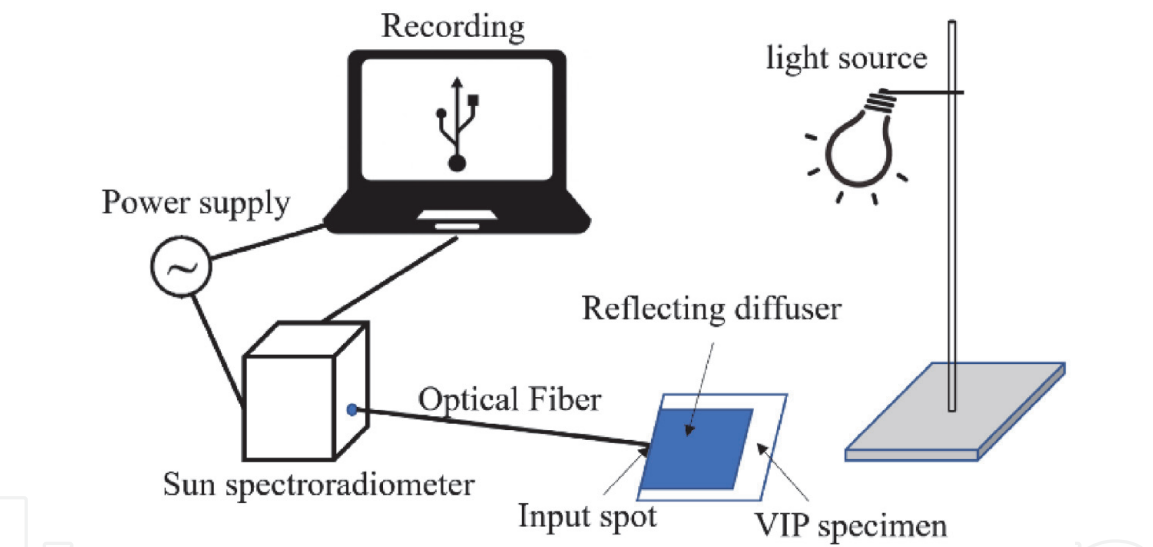


**Figure 19.**
*Trial manufacturing methods for the frame-type VIP (a) normal method with calcium oxide adsorbent, (b) using vacuum drying chamber with N₂, (c) using flat silicon rubber heaters during the evacuation, and (d) using gas adsorbent getter [6].*

oxide pack. The results were recorded for 75 h and are showed in **Figure 20b** [6]. The results showed that using getter material attained a lower panel effective thermal conductivity compared to using calcium oxide desiccant packs. The



**Figure 20.**
*Variation of the center-of-panel thermal conductivity with the elapsed time for (a) different trial manufacturing methods and (b) two different outgassing adsorbent materials [6].*



**Figure 21.**
*Experimental apparatus used in the estimation of the VIP thermal conductivity: (a) Schematic diagram, (b) real images of the used test apparatus, and (c) real images of the used peek, frame, and mesh VIPs and the transparent gas barrier film [6].*

minimum achieved thermal conductivity was about 0.011 W/m K, and this value corresponds to 5 Pa in the case of using getter. This clarifies that the VIP inner pressure is increased after the sealing, because of core material outgassing.

### 4.1.3 Heat flux meter method (simultaneous evacuation thermal conductivity measurement)

**Figure 21** shows the simultaneous evacuation thermal conductivity measurement applying HFM method [6]. This technique achieves evacuation with simultaneous measuring of the thermal conductivity. In this experimental setup, the vacuum pump is connected with the experiments of the heat flow meter (HFM). Three sides of the VIP were sealed thermally using the large width sealing in the vacuum sealing machine. The width of the sealing was 9 mm. Then, fourth edge of the envelope is kept connected to the hose/pipe of a small-scale vacuum pump. The experimental setups are showed in **Figure 21**. The vacuum pump in this setup consists of two vacuum pumps. One is a series connected reciprocating and turbomolecular vacuum pump. Pirani pressure gauge is used to measure the VIP inner pressure. The VIP and the sensor used for pressure measurement can be easily isolated from the system by the mean of valve. The experiment starts with operating the reciprocating pump to



**Figure 22.**
*Schematic representation for the illuminance measurement [6].*

| Conditions | Without VIP | Silica aerogel spacer | Peek type spacer | Mesh-type spacer | Frame-type spacer |
|---|---|---|---|---|---|
| Intensity ($\mu W/cm^2/nm$) | 20000 | 14000 | 17500 | 13000 | 15000 |
| Transparency Ratio | 1 | 0.70 | 0.88 | 0.65 | 0.75 |

**Table 4.**
*Measured transparency for the experimentally examined VIPs [6].*

decrease the VIP inner pressure to around 20 Pa. Then, the turbomolecular pump is operated to decrease the inner pressure until reaching the desired value. The turbomolecular vacuum pump with the oil free type is favorable for these applications, as suggested by [18]. The pressure sensing device was located closer to the inlet part of the VIP; this allows us to precisely measure the pressure inside the VIP. After reaching the desired vacuum level, the VIP sample is inserted into the HFM apparatus. The measurement of thermal conductivity is the same as the normal HFM method. Examples of experimental results are indicated in **Figure 13a–c**.

## 4.2 Transparency

The light transparency experiment is described in **Figure 22** [6]. In this experiment, the TVIP sample is positioned on a reflection diffuser. Then the TVIP sample is irradiated using incandescent light lamp. An 800-nm wavelength was measured and the illuminance intensity in $\mu W/(cm^2 \, nm)$ is measured with and without the TVIP shading. The transparency percentage is defined as the ratio between the measured value of the transmitted light intensity while using the TVIP the same value while not including the TVIP.

**Table 4** shows the transparency percentage of all the fabricated TVIPs [6]. These transparency percentage is the TVIPs without the glass window of 3 mm. It is obvious that the transparency values for the manufactured VIPs vary between 0.65 and 0.9, for mesh-type and the cylindrical-pillar VIPs, respectively. Further, because the modified peek spacer was studied numerically, the predictable transparency could be similar to that of the peek type spacer.

## 5. Additional performance analysis of transparent vacuum insulation panels

### 5.1 Thermal performance analysis under American Society for Testing and Materials (ASTM) boundary conditions

A 3D model is developed and solved for the investigated TVIPs while they attached to a 3 mm glass layer thick. The temperature contours on both the cold and hot sides, heat flux, and U-value of the VIP samples were predicted at the ASTM boundary conditions. In ASTM boundary conditions, the indoor air temperature and the convection heat transfer coefficients were 21.1°C and 8.3 W/m$^2$ K while the same for the outdoor conditions were −17.8°C and 30 W/m$^2$ K, respectively.

The 3D temperature contours on the vacuum region at a vacuum pressure of 0.1 Pa are depicted in **Figure 23**. **Figure 23** shows a considerable temperature difference exists among the two sides of the vacuum gap. The maximum temperature difference was for the mesh-type spacer. Further, using the mesh-type VIP with 3-mm glass decreases the center of pane U-value from 6.3 to 1.14 W/m$^2$ K. This considerable decrease in the U-value declines the heat loss from the indoor environment of the building. Furthermore, using silica aerogel-based VIP, higher U-value was obtained. This due to the high heat is transfer rate through the silica aerogel spacer.

### 5.2 Annual energy analysis

The hourly variation and total annual thermal energy transferred through the proposed VIP to the indoor environment is calculated, analyzed, and compared with the customary window without VIP. The VIP is attached to the 1 m$^2$
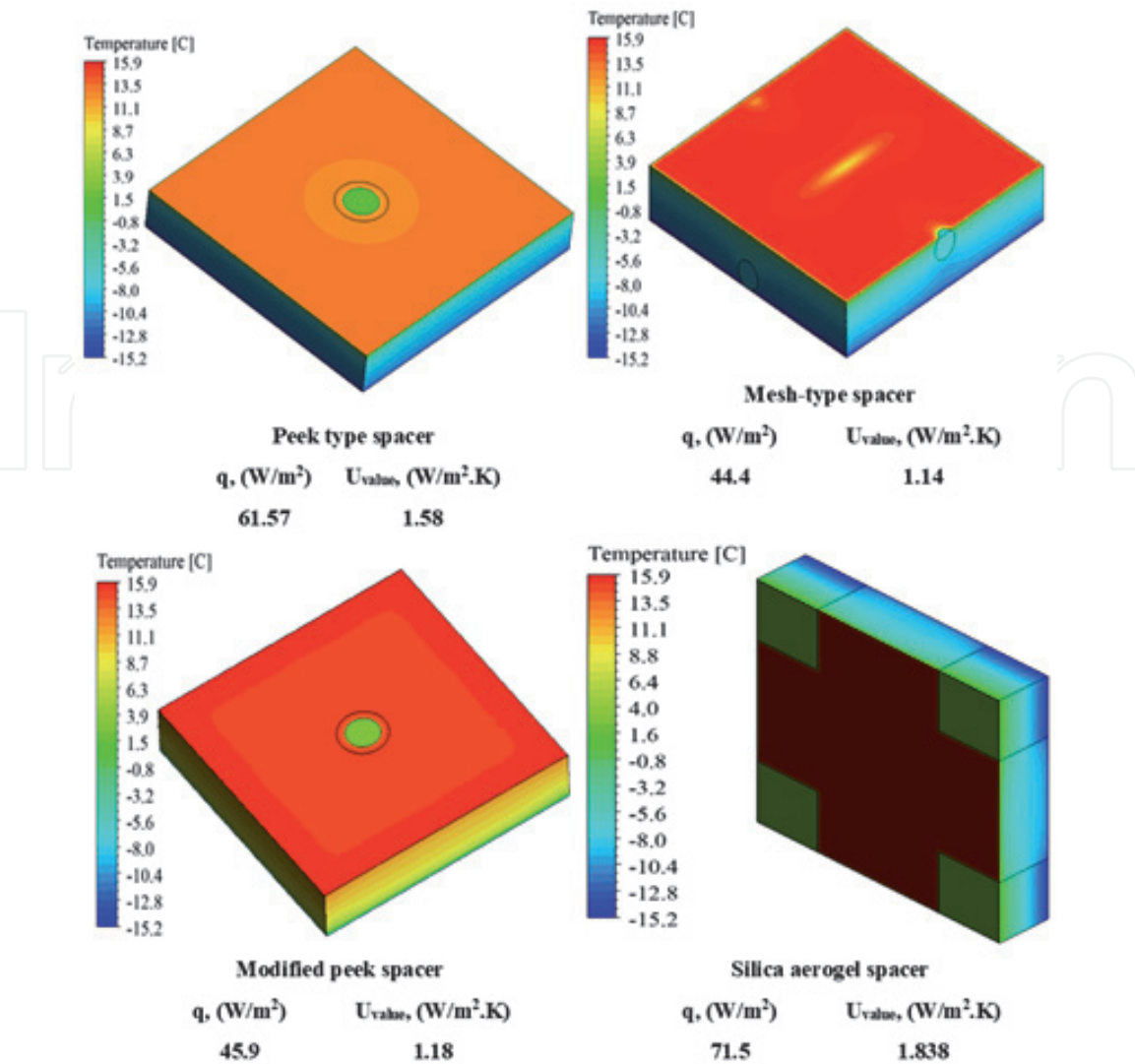
**Figure 23.**
*Predicted 3D temperature contours of the investigated VIPs using American Society for Testing and Materials (ASTM) boundary conditions [6].*

single-layered glass window with 3 mm thickness. In this calculation, the indoor air temperature is at 20°C, with an indoor convective heat transfer coefficient (HTC) of 7.7 W/m$^2$ K as recommended by Refs. [18, 20]. In addition, two typical climate conditions at Ishigaki island (24.41°N, 124.17°E) as a hot region, and Sapporo, Hokkaido (43.06°N, 141.35°E) as a cold region are examined in Japan. **Figure 20a** and **b** show the hourly variation of ambient temperature and wind speed, respectively. These meteorological conditions at Ishigaki city are measured by the authors, and that for Sapporo was downloaded from Japan Meteorological Agency website. In-house MATLAB code is developed to estimate the hourly and the annual thermal energy transfer. The minimum ambient temperature in Sapporo city is −10°C while the maximum air temperature in Ishigaki island is 32°C.

The model adopted in this section is a one-dimensional quasi-steady model. This model is an efficient for a long-term energy evaluation, as it predicts results with reasonably accepted accuracy in a short period of time.

In this model, the following assumptions are applied:

1. The heat transferred in one-dimensional and under a quasi-steady state condition.

2. The effect of the contact thermal resistance between the VIP and the glass window is neglected.

3. The impact of sol-air is not considered as we assume that no solar radiation strikes the exterior surface of the window.

The steady-state conduction heat flux transfer through the VIP-glass window system to the indoor space is calculated by Eq. (9):

$$q = \frac{(T_a(t) - T_i)}{\left(\frac{1}{h_{c,i}} + \frac{\delta_g}{k_g} + \frac{\delta_v}{k_v} + \frac{1}{h_{c,o}(t)}\right)} \qquad (9)$$

where, $q$, $\delta_g$, $k_g$, $\delta_v$, $k_v$, and $h_{c,i}$ are the total thermal heat flux in W/m², glass thickness in m, glass thermal conductivity in W/m K, VIP thickness in m, VIP thermal conductivity in W/m K, and the inside convective heat transfer coefficient in W/m² K, respectively. Please note that the negative sign of $q$ indicates that the heat loss from the building, which occurs when the outside temperature is less than the indoor designated temperature. The outdoor convective HTC variation with time is calculated as a function of wind speed and ambient temperature according to ambient temperature-dependent equation derived by Nusselt-Jürges [21]. This equation is written for smooth surfaces, such as the exterior surfaces of windows, as shown in Eqs. (10) and (11) [21]:

$$h_{c,o}(t) = 5.678 \left\{ 0.99 + 0.21 \times \left[ \left(\frac{294.26}{273.16 + T_a(t)}\right) \times \frac{U_\infty(t)}{0.3048} \right] \right\} \ at \ U_\infty(t) < 4.88 \left(\frac{m}{s}\right)$$

$$(10)$$

$$h_{c,o}(t) = 5.678 \left\{ 0.5 \times \left[ \left(\frac{294.26}{273.16 + T_a(t)}\right) \times \frac{U_\infty(t)}{0.3048} \right]^{0.78} \right\} \ at \ 4.88 \leq U_\infty(t) < 30.48 \left(\frac{m}{s}\right)$$

$$(11)$$

Here, $h_{c,o}(t)$, $T_a$ (t), and $U_\infty(t)$ are the hourly convective HTC at the exterior surfaces of the window in W/m² K, the hourly ambient temperature variation with the time in °C, and the hourly wind speed in m/s, respectively. The constants in Eqs. (10) and (11) are empirical constants derived from the experiments developed by Nusselt-Jürges. **Table 5** lists the thicknesses of the VIPs with the relevant thermal conductivities at a pressure of 1 Pa for different spacers [6].

The hourly variation of the heat flux for the single-layered glass window without/with a frame-type VIP attached to the internal surface of a glass window is shown in **Figure 24a** and **b** for Sapporo and Ishigaki, respectively [6]. These two figures show that attaching the VIP to the single-layer glass windows of existing buildings can reduce the heat loss/gain from/to the building in cold and hot weather conditions, respectively. Hence, it is highly recommended to use the VIP in cold regions such as Sapporo, where the temperature difference between the outside ambient temperature and the inside designed conditions can reach to maximum value of 30°C.

| | Peek spacer | Mesh spacer | Cylindrical pillar | Frame spacer | Modified peek spacer | Silica aerogel |
|---|---|---|---|---|---|---|
| Thickness, (mm) | 4.5 | 2 | 4.5 | 3 | 4.5 | 4 |
| $k_v$ @1 Pa, (mW/m.K) | 14.2 | 6.5 | 16.7 | 6.8 | 12.4 | 17.7 |

**Table 5.**
*Detailed thickness and center-of-panel thermal conductivities of the investigated VIPs at 1 Pa [6].*
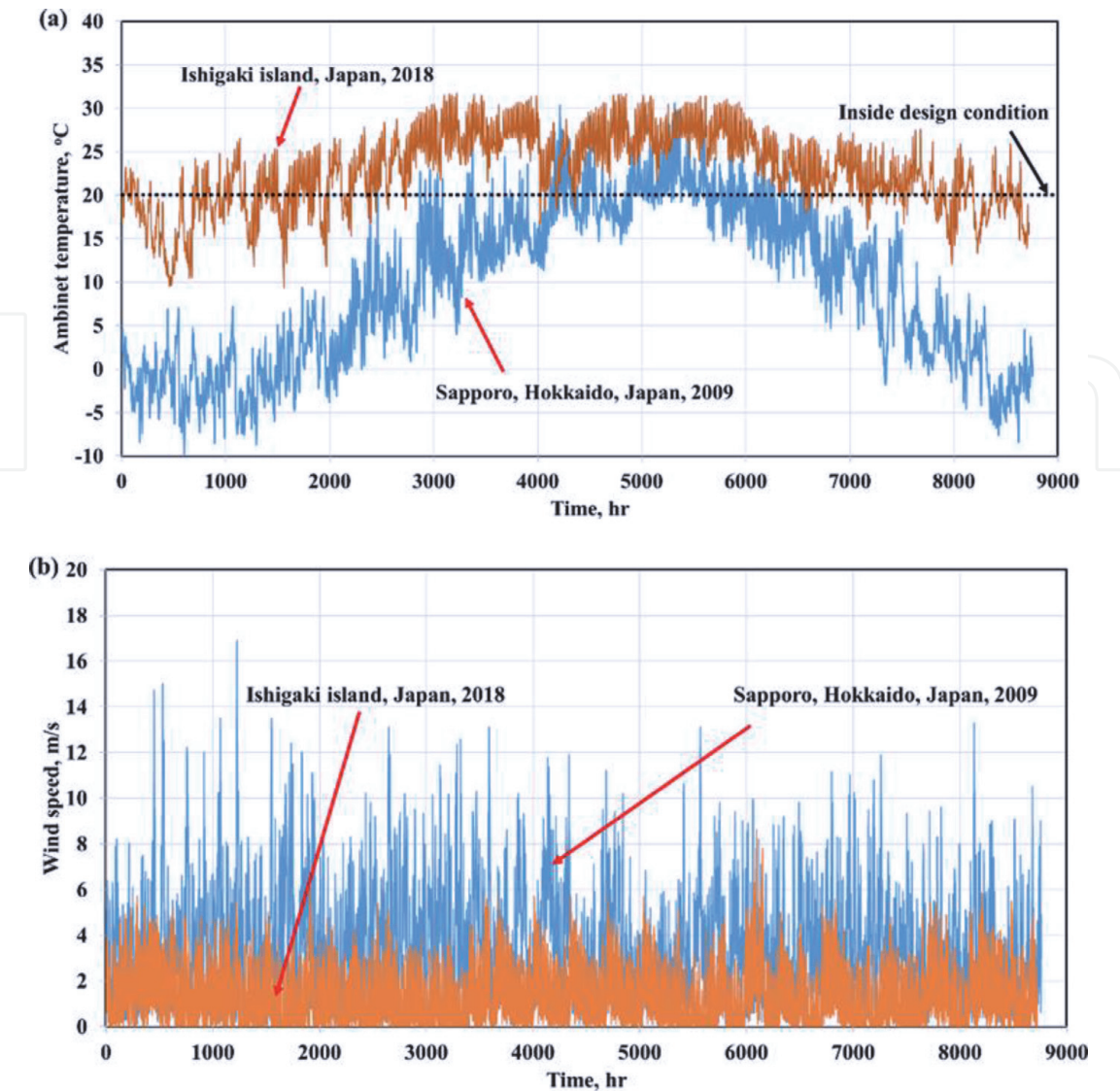
**Figure 24.**
*Hourly variation of (a) ambient temperature and (b) wind speed for Ishigaki and Sapporo cities in Japan [6].*

The hourly variation of the thermal heat flux in $W/m^2$ for a single layer window with/without VIP under climate conditions of Ishigaki Island and Sapporo city are displayed in the **Figure 25**, While, the total thermal energy transfer per unit floor area per annum in $kW\,h/m^2/annum$ is calculated and compared for all VIPs with different spacer structure is illustrated in **Figure 26a** and **b** for Sapporo and Ishigaki, respectively [6]. First, the total annual heat flux in $W/m^2/annum$ is the summation of loss and gain heat transfer. For the Sapporo region, it is obvious that the total annual heat flux loss is dominant heat transfer occurred in this region, owing to the cold weather. In addition, attaching a frame VIP to the inside surface of a customary 3-mm glass window reduces the heat loss from the buildings by 69.5% compared with the typical window without VIP. In contrast, for Ishigaki region, the heat gain from the window has a significate share of the total heat transfer rate, and a 65.1% decrement in the annual heat gain is accomplished by using the VIP combined with 3-mm glass windows.

## 6. Summary

New, low-cost transparent vacuum insulation panels (TVIPs) using structured cores are proposed. These TVIPs are different from the well-known conventional
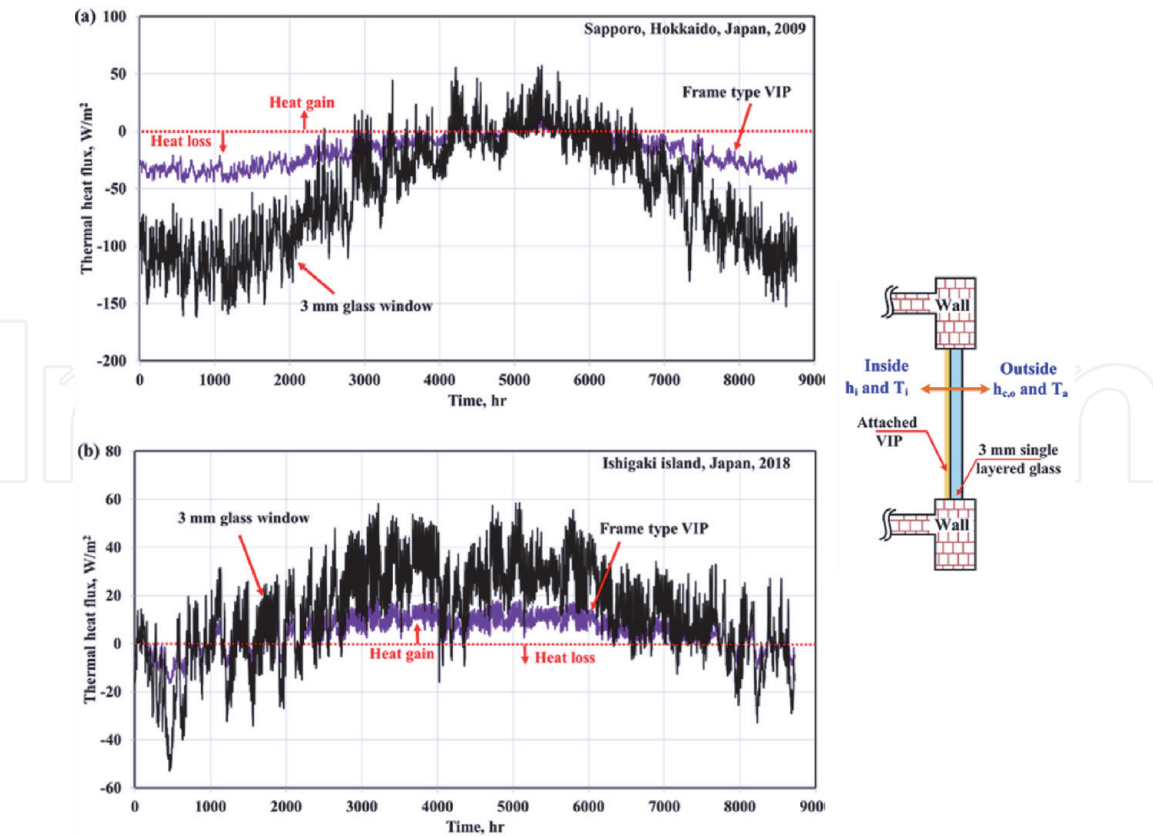
**Figure 25.**
*Hourly variation of the thermal heat flux transfer in W/m² for (a) Sapporo and (b) Ishigaki in the case of using single-layered glass window and the frame-type VIP attached to the glass window as an example. The VIP with the glass window is displayed at the right of the figure [6].*
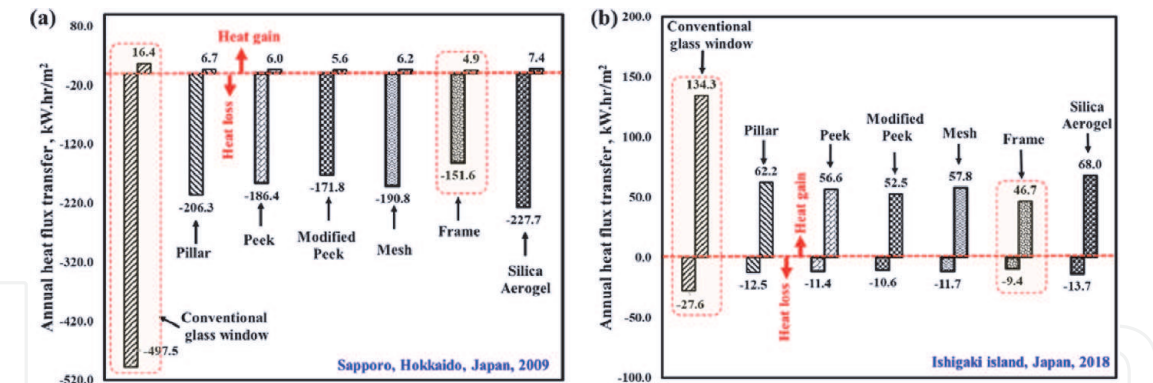


**Figure 26.**
*Variation of the total annual heat flux transfer in a unit of kW h/m² for (a) Sapporo and (b) Ishigaki region [6].*

VIP, which has a solid core material structure and opaque metalized film barrier envelope. The proposed novel TVIPs are showed a high thermal insulation capability, which could attached to the windows of existing buildings. The five spacers, which are namely peek, modified peek, mesh, silica aerogel, and frame, are selected as the structured core. Numerical simulations are developed to evaluate the effective thermal conductivity of TVIPs with five different spacers at different pressure levels, and the results are compared to the experimental pairs. The results indicate that the frame-type spacer with a thickness of 3 and 2 mm attain the lowest center-of-panel thermal conductivities of $6.5 \times 10^{-3}$, it followed by the mesh-type spacer, which achieved a value of $6.8 \times 10^{-3}$ W/m K at a vacuum pressure of 1 Pa, respectively. The predicted U-values for the mesh spacers was 1.14 W/m² K at ASTM boundary conditions. Moreover, attaching a frame-type TVIP with a

thickness of 3 mm to an existing window decreases the space heat loss by approximately 69.5%.

The TVIPs have the significant potential to promote thermal insulation capability of the windows of existing buildings with low cost. On the other hand, the challenge of TVIPs is to keep the low pressure inside the envelope after vacuum sealing. As shown in the result of thermal conductivity measurement applying HFM method and using a TVIP after vacuum sealing, the apparent thermal conductivity is increasing according to elapsed time. The reason should be due to the outgassing from the core material; therefore, it is important to reduce the outgassing to realize the TVIPs.

## Acknowledgements

## Conflict of interest

The authors declare no conflict of interest.

## Nomenclature

| | |
|---|---|
| $A$ | vacuum insulation panel front area (m$^2$) |
| $a$ | length of span (m) |
| $E$ | emissive power density (W/m$^2$), |
| $E_y$ | Young's modulus (Pa) |
| $h_{c,i}$ | convection heat transfer coefficient to building interior [W/(m$^2$ K)] |
| $h_{c,o}$ | convective heat transfer coefficient to building exterior [W/(m$^2$ K)] |
| $k$ | thermal conductivity [W/(m K)] |
| $L_v$ | transparent VIP thickness (m) |
| $P$ | vacuum pressure (N/m$^2$) |
| $R$ | thermal resistance [(m$^2$ K)/W] |
| $q$ | heat flux (W/m$^2$) |
| $T$ | temperature (°C) |
| $U_\infty$ | wind speed (m/s) |

### Greek symbols

| | |
|---|---|
| $\Delta$ | difference |
| $\delta$ | thickness (m) |
| $\varepsilon$ | emissivity (unitless) |
| $\lambda_o$ | air thermal conductivity [W/(m K)] |
| $\lambda_v$ | vacuum space thermal conductivity [W/(m K)] |

| | |
|---|---|
| $\mu$ | Poisson's ratio |
| $\sigma$ | coefficient of uniform loading to a rectangular flat plate |
| $\omega$ | deflection (m) |

## Subscripts

| | |
|---|---|
| $a$ | ambient |
| $avg$ | average |
| $c$ | VIP cold side |
| $eff$ | effective |
| $g$ | glass |
| $h$ | VIP hot side |
| $h\text{-}c$ | between the hot and the cold side of the VIP |
| $i$ | interior |
| $in$ | entering the surface |
| $m$ | measured |
| $out$ | exiting from the surface |
| $VIP$ | VIP |
| $v$ | vacuum space |
| $v_1, v_2, v_3$ | vacuum layer |

## Author details

Takao Katsura
Hokkaido University, Sapporo, Japan

*Address all correspondence to: katsura@eng.hokudai.ac.jp

IntechOpen

## References

[1] Fricke J, Heinemann U, Ebert HP. Vacuum insulation panels—From research to market. Vacuum. 2008;**82**: 680-690. DOI: 10.1016/j. vacuum.2007.10.014

[2] Boafo FE, Kim J-H, Kim J-T. Numerical study of slim curtain wall spandrel with integrated vacuum insulation panel: Concept, performance evaluation and challenges. Energy and Buildings. 2019;**183**:139-150. DOI: 10.1016/j.enbuild.2018.10.036

[3] Yang Z, Katsura T, Aihara M, Nakamura M, Nagano K. Development of numerical heat transfer and the structural model to design slim and translucent vacuum layer type insulation panels to retrofitting insulation in existing buildings. Energies. 2017;**10**. DOI: 10.3390/ en10122108

[4] Fantucci S, Garbaccio S, Lorenzati A, Perino M. Thermo-economic analysis of building energy retrofits using VIP-vacuum insulation panels. Energy and Buildings. 2019;**196**:269-279. DOI: 10.1016/j.enbuild.2019.05.019

[5] Buratti C, Moretti E, Zinzi M. High energy-efficient windows with silica aerogel for building refurbishment: Experimental characterization and preliminary simulations in different climate conditions. Buildings. 2017. DOI: 10.3390/buildings7010008

[6] Katsura T, Radwan A, Yang Z, Nakamura M, Nagano K. Energy conservation using new structured-core and transparent vacuum insulation panels: Numerical simulation with experimental validation. Solar Energy. 2019;**193**:885-905. DOI: 10.1016/j. solener.2019.09.083

[7] Yang Z, Katsura T, Aihara M, Nakamura M, Nagano K. Investigation into window insulation retrofitting of existing buildings using thin and translucent frame-structure vacuum insulation panels. Energies. 2018;**11**. DOI: 10.3390/en11020298

[8] Timoshenko S, Woinowsky-Krieger S. Theory of Plate and Shell. Columbus, OH, USA: McGraw-Hill Book Company; 1959. pp. 106-108

[9] Young WC, Budynas RG. Roark's Formulas for Stress and Strain. 7th ed. New York, NY, USA: McGraw-Hill Professional; 2001. pp. 508-509

[10] Baetens R, Jelle BP, Thue JV, Tenpierik MJ, Grynning S, Uvsløkk S, et al. Vacuum insulation panels for building applications: A review and beyond. Energy and Buildings. 2010;**42**: 147-172. DOI: 10.1016/j. enbuild.2009.09.005

[11] Arya F, Moss R, Hyde T, Shire S, Henshall P, Eames P. Vacuum enclosures for solar thermal panels. Part 1: Fabrication and hot-box testing. Solar Energy. 2018;**174**:1212-1223. DOI: 10.1016/j.solener.2018.10.064

[12] Arya F, Moss R, Hyde T, Shire S, Henshall P, Eames P. Vacuum enclosures for solar thermal panels. Part 2: Fabrication and hot-box testing. Solar Energy. 2018:1212-1223. DOI: 10.1016/j. solener.2018.10.064

[13] Choi B, Yeo I, Lee J, Kang WK, Song TH. Pillar-supported vacuum insulation panel with multi-layered filler material. International Journal of Heat and Mass Transfer. 2016;**102**:902-910. DOI: 10.1016/j.ijheatmasstransfer.2016. 06.032

[14] ANSYS FLUENT Theory Guide; 2011

[15] Kim J, Song TH. Vacuum insulation properties of glass wool and opacified fumed silica under variable pressing

load and vacuum level. International Journal of Heat and Mass Transfer. 2013;**64**:783-791. DOI: 10.1016/j. ijheatmasstransfer.2013.05.012

[16] Fang Y, Eames PC, Norton B, Hyde TJ. Experimental validation of a numerical model for heat transfer in vacuum glazing. Solar Energy. 2006;**80**: 564-577. DOI: 10.1016/j. solener.2005.04.002

[17] Fang Y, Hyde T, Hewitt N, Eames PC, Norton B. Comparison of vacuum glazing thermal performance predicted using two- and three-dimensional models and their experimental validation. Solar Energy Materials & Solar Cells. 2009;**93**: 1492-1498. DOI: 10.1016/j. solmat.2009.03.025

[18] Memon S, Fang Y, Eames PC. The influence of low-temperature surface induction on evacuation, pump-out hole sealing and thermal performance of composite edge-sealed vacuum insulated glazing. Renewable Energy. 2019;**135**:450-464. DOI: 10.1016/j. renene.2018.12.025

[19] Katsura T, Yang Z, Aihara M, Nakamura M, Nagano K. Development of slim and translucent vacuum insulation panels. Journal of Japan Solar Energy Society. 2018;**44**:49-57. DOI: 10.24632/jses.44.2_49

[20] Fang Y, Hyde TJ, Hewitt N. Predicted thermal performance of triple vacuum glazing. Solar Energy. 2010;**84**: 2132-2139. DOI: 10.1016/j. solener.2010.09.002

[21] Palyvos JA. A survey of wind convection coefficient correlations for building envelope energy systems' modeling. Applied Thermal Engineering. 2008;**28**:801-808. DOI: 10.1016/j.applthermaleng.2007.12.005